8462–8470 *Nucleic Acids Research, 2021, Vol. 49, No. 15* *Published online 6 August 2021*
https://doi.org/10.1093/nar/gkab650

A small-molecule fluorescence probe ANP77 for sensing RNA internal loop of C, U and A/CC motifs and their binding molecules

Bimolendu Das, Asako Murata and Kazuhiko Nakatani*

Department of Regulatory Bioorganic Chemistry, SANKEN (The Institute of Scientific and Industrial Research), Osaka University, 8-1 Mihogaoka, Ibaraki, Osaka 567-0047, Japan

Received December 11, 2020; Revised July 02, 2021; Editorial Decision July 19, 2021; Accepted August 04, 2021

ABSTRACT

Small-molecules interacting with particular RNAs and modulating their functions are vital tools for RNA-targeting drug discovery. Considering the substantial distribution of the internal loops involving two contiguous cytosines opposite to a single-nucleotide base (Y/CC; Y = C, U or A) within the biologically significant functional RNAs, developing small-molecule probes targeting Y/CC sites should provide profound insight into their functions and roles in biochemical processes. Herein, we report ANP77 as the small-molecule probe for sensing RNA internal loop of Y/CC motifs and molecules binding to the motifs. The Y/CC motifs interact with ANP77 via the formation of a 1:1 complex and quench the fluorescence of ANP77. The flanking sequence-dependent binding to C/CC and U/CC sites was assessed by fluorometric screening, provided the binding heat maps. The quenching phenomena of ANP77 fluorescence was confirmed with intrinsic potential drug target pre-miR-1908. Finally, the binding-dependent fluorescence quenching of ANP77 was utilized in the fluorescence indicator displacement assay to demonstrate the potential of ANP77 as an indicator by using the RNA-binding drugs, risdiplam and branaplam.

GRAPHICAL ABSTRACT

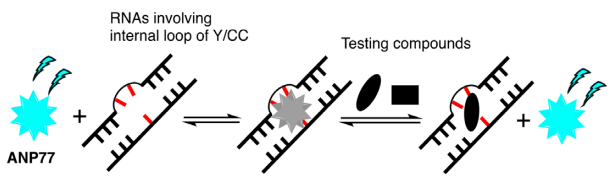

INTRODUCTION

Besides the transduction of genetic information, RNAs regulate gene expression and play a key role in many biological processes, particularly in developing human diseases (1,2). Site-specific interaction and modulation of RNA functions by small-molecule become an attractive and growing strategy for RNA drug hunters (3–5). Towards this end, several RNA binding ligands have been studied by targeting structurally fluctuated sites involving hairpin loops, internal loops and bulged sites (6–9). Among these structural elements in RNAs, internal loops in higher-order structures of viral RNAs (10), ribosomal RNAs (11) and RNAs of repeats associated disorders (8,9,12,13) were demonstrated as significant motifs for small-molecule drugs. Also, internal loops are the key structural feature of the precursors of micro-RNAs (miRs). MiRs are small single-stranded RNAs (a length of 19−25 nucleotides) produced by successive enzymatic digestions of primary-miR. MiRs regulate gene expression and cause many diseases on their dysregulation (14–16). Targeting internal loops in the miR precursors by small-molecule is a potential approach to gain profound insight into the miR biogenesis and eventually develop drugs towards therapeutics (17–19).

For discovering new molecules targeting RNAs, the fluorescence indicator displacement (FID) technique offers a promising potential (20–22). In brief, FID is based on the quenching of molecular fluorescence by the binding to the targets, i.e. RNA in these studies. The indicators' quenched fluorescence would be restored if the indicators were displaced by the external molecules and dissociated from the targets. Increasing fluorescence by adding the external molecules to the mixture of target RNA and indicator determines the compounds' competitive binding with the indicator molecule. There are two types of fluorescence indicators. One is a general indicator without high sequence and structural preference (22–25) and the other with high selectivity (21,26,27). In principle, fluorescence indicators without high sequence and motif selectivity are useful probes for screening against variety of targets in the wide concentration range but suffer from the possibility in

*To whom correspondence should be addressed. Tel: +81 6 6879 8455; Fax: +81 6 6879 8459; Email: nakatani@sanken.osaka-u.ac.jp

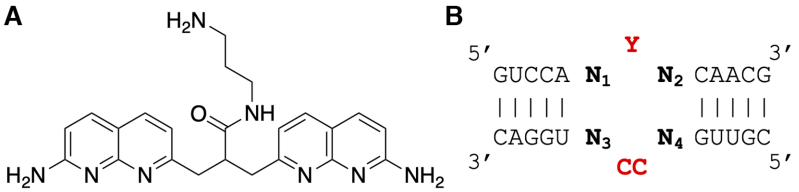

Figure 1. (**A**) Structure of **ANP77**. (**B**) dsRNAs involving the internal loop motifs of Y/CC (red type) with all possible nearest neighbor base pairing (bold type) used in this study; N_1-N_3 and N_2-N_4 are any combination of A, C, G and U.

multiple binding to the target leading to the decrease in the fluorescence change and, therefore, the accuracy of screening results. In contrast, indicators with high sequence and motif selectivity would be ideal for the FID assay to screen out the molecules targeting the indicator-binding site. Although the utility of the indicators is rather limited to the sequence and motifs, the indicator can be used for weak binding target with appropriate evaluation of fluorescence changes. Therefore, for the success of FID assay the use of several indicators showing different fluorescence quenching and binding properties would be useful. In this regard, development of sequence and motif selective indicator would be critical to improve the assay quality. Studies so far focused on this direction are limited to the fluorophore-conjugates of RNA binding aminoglycosides and peptides (21,26,27). In our continuous efforts on developing small molecules targeting specific nucleic acid sequences and motifs involving bulges and mismatches (28), we discovered several fluorescent molecules, which are the derivatives of xanthone (20,29) and naphthyridine (30,31). Xanthones were utilized as an indicator to identify small molecules that bind to the IIB domain of HIV-1 Rev Response Element RNA and miR precursors (20,32,33), whereas 2-amino or 2,7-diamino derivatives of 1,8-naphthyridine, as a probe for single nucleotide cytosine-bulge (C-bulge) (30,34,35) and C-C mismatch site of nucleic acids (31,36). Herein, we report a dimeric molecule of 2-amino-1,8-naphthyridine named **ANP77** (*N*-3-aminopropyl-1,3-bis(2-**a**mino-1,8-**n**aphthyridin-7-yl)**p**ropane-2-carboxamide) (Figure 1A) as a novel fluorescent probe, selective for the internal loop of Y/CC motifs in RNAs structure (Figure 1B) and studied its potential as a fluorescence indicator to discover Y/CC motif binding molecules by FID assay. The binding-dependent fluorescence quenching of **ANP77** was utilized in the FID assay to demonstrate the potential of **ANP77** as an indicator by using the RNA-binding drugs branaplam (37) and risdiplam (38), which have been developed to treat spinal muscular atrophy (SMA) (39). As per the miRbase database (http://www.mirbase.org/) (40), internal loops of Y/CC motifs represent one of the critical secondary structural components of several biologically significant functional miRs precursors (Supplementary Figures S1–S3) (40–42).

MATERIALS AND METHODS

Synthesis of ANP77

ANP77 was synthesized as described before (43), and the synthetic scheme shown in Supplementary Scheme S1.

Melting temperature (T_m) measurements

Thermal denaturation profiles of the RNA duplexes (5 μM) with or without **ANP77** (25 μM) in sodium cacodylate buffer (10 mM, pH 7) containing sodium chloride (100 mM) were recorded on a UV-2700 spectrophotometer (Shimadzu) equipped with a TMSPC-8 temperature controller and a 1 cm path-length cell. The absorbance of the samples was monitored at 260 nm from 2°C to 85°C with a heating rate of 1°C /min. T_m values were calculated by the median method. RNAs used were procured from Gene Design Inc. (Osaka, Japan).

CSI-TOF-MS measurements

Time-of-flight mass spectrometry analysis by cold spray ionization (CSI-TOF MS) data were measured on JEOL JMS-T100LP AccuTOF LC-plus 4G mass spectrometer in negative mode. Samples containing RNA duplex r(C/CC) [r(C): 5′-r(GUC CAG **C** GCA ACG)-3′ / r(CC): 3′-r(CAG GUC **CC** CGU UGC)-5′] (10 μM) with or without **ANP77** (50 μM) in 1:1 mixture of water and methanol containing ammonium acetate (50 mM) were sprayed at a flow rate of 14 μl min^{-1}. Spray temperature was fixed at –10°C during the injection.

Isothermal titration calorimetry measurements

Isothermal titration calorimetry (ITC) experiments were carried out at 25°C on a MicroCal iTC200 calorimeter. A 40 μl injection syringe containing **ANP77** (30 μM) solution in aqueous 10 mM sodium cacodylate (pH 7) and 100 mM NaCl was titrated into a cell containing 250 μl solution of RNA duplex r(Y/CC) [r(Y): 5′-r(GUC CAG **Y** GCA ACG)-3′ / r(CC): 3′-r(CAG GUC **CC** CGU UGC)-5′] (2 μM) in 10 mM sodium cacodylate (pH 7) and 100 mM NaCl. Titrations typically consisted of a total of 19 injections (0.4 μl for the first injection and 2 μl for the remaining injections) of 4 s duration each, with 160 s delay between the injections. Data from the first injection were discarded before analysis. Analysis of the data was performed with Origin 7.0 software (MicroCal). The binding isotherms thus obtained were fitted to a one-set-of-sites model to calculate reaction stoichiometry (n), association constant (K_a), enthalpy (ΔH) and entropy (ΔS).

Measurements of fluorescence spectra

Fluorescence spectra of **ANP77** in the presence and absence of RNA duplex or pre-miR-1908 in sodium cacodylate buffer (10 mM, pH 7) and 100 mM NaCl were measured

at room temperature using JASCO FP-8500 spectrofluorometer with a 10 mm optical path-length cell or a microcell of path-length 3 mm. The samples were excited at the maximum absorption wavelength of **ANP77** (334 nm) with a slit width of 2.5 nm and a response time of 0.5 s. The apparent quenching efficiency (Q_{app}) of RNAs was calculated by the Equation (1):

$$Q_{app} = [(F_0 - F_{obs}) / (F_0 - F_{blank})] \times 100\% \quad (1)$$

where F_0 is fluorescence intensity of **ANP77** without RNA, F_{obs} is fluorescence intensity of **ANP77** in the presence of RNA, and F_{blank} is fluorescence of the cuvette (or well) containing buffer. For the measurements of fluorescence with spectrophotometer, F_{blank} was assumed to be zero to calculate Q_{app}. Fluorescence intensities are obtained as peak intensity at a wavelength of 389 nm (emission maxima of **ANP77**).

Fluorometric screening

The fluorometric screening was performed with equimolar mixture (1 μM) of **ANP77** and dsRNA in sodium cacodylate buffer (10 mM, pH 7) and sodium chloride (100 mM) using a 384-well assay plate. The fluorescence of each well containing sample (15 μl volume) was measured using a microplate reader (Mithras LB 940) with 355 nm excitation and 410 nm emission filters at room temperature. Samples lacking the RNA duplex or both dsRNA and **ANP77** was also dispensed to the plate and measured the fluorescence. All of the RNAs used for the fluorometric screening were procured from Gene Design Inc. (Osaka, Japan). For the calculation of Q_{app} with the plate reader measurements, F_{blank} is the fluorescence of the well containing buffer, i.e. sample lacking both dsRNA and **ANP77**.

Fluorescence indicator displacement (FID)

The FID study was carried out by measuring the fluorescence spectra of **ANP77** (0.25 μM) with r(Y/CC) (0.5 μM) in the presence and absence of RNA splicing modifier drug molecules (10 μM) (Branaplam or Risdiplam) containing 1% DMSO in sodium cacodylate buffer (10 mM, pH 7) and sodium chloride (100 mM) at room temperature using JASCO FP-8500 spectrofluorometer and a micro-cell of path-length 3 mm. The samples were excited at a wavelength of 334 nm with a slit width of 2.5 nm and setting the response time of 0.5 s. FID titrations were carried out by measuring the fluorescence spectra of **ANP77** (0.25 μM) and r(Y/CC) (0.5 μM) in the presence of various concentrations of drug molecules. Drug molecules Branaplam and Risdiplam were purchased from MedChemExpress Co. Limited and Neomycin was purchased from Sigma-Aldrich as Neomycin trisulfate salt hydrate.

Fluorescence recovery of **ANP77** (F_{rec}) (%) was calculated by the Equation (2):

$$F_{rec} = \left[\left(F' - F_{obs}\right) / (F_0 - F_{obs})\right] \times 100\% \quad (2)$$

where F_0 = fluorescence intensity of **ANP77**, F_{obs} = fluorescence intensity of **ANP77** in presence of r(Y/CC), F' = fluorescence intensity of **ANP77** with r(Y/CC) in the presence of drug molecule (branaplam or risdiplam or neomycin). Fluorescence intensities are monitored at the emission maxima wavelength of **ANP77** (389 nm) and the data presented are average of three independent experiments.

The Z'-factor was calculated using the following Equation (3) under the FID experiment conditions by considering the fluorescence of **ANP77** as high-value signal and the fluorescence of **ANP77** in the presence of Y/CC as low-value signal (44,45):

$$Z' - \text{factor} = 1 - 3 \times (\sigma_{hs} + \sigma_{ls}) / |\mu_{hs} - \mu_{ls}| \quad (3)$$

where μ and σ represent mean and standard deviation, respectively, and 'hs' indicates high-value signal and 'ls' indicates low-value signal.

To estimate Z'-factor for screening with plate reader, we utilized 384 well plate employing **ANP77** (1 μM) (using 24 wells, 15 μl sample solution in each well) and mixture of **ANP77** and r(C/CC) (1 μM each) (using 24 wells, 15 μl sample solution in each well) in sodium cacodylate buffer (10 mM, pH 7) and sodium chloride (100 mM). The fluorescence of each sample well was measured using a microplate reader (Mithras LB 940) with 355 nm excitation and 410 nm emission filters at room temperature. μ_{hs} and σ_{hs} calculated from the 24 wells of **ANP77** as 12005 and 306, respectively. μ_{ls} and σ_{ls} calculated from the 24 wells of the mixture of **ANP77** and r(C/CC) as 5992 and 372, respectively.

Circular dichroism measurements

Circular dichroism (CD) experiments were carried out on a J-725 CD spectrometer (JASCO) using a 10 mm path length cell at room temperature. CD spectra of pre-miR-1908 (1 μM) were measured with sodium cacodylate buffer (10 mM, pH 7) containing NaCl (100 mM) in the absence and presence of **ANP77** (25 μM).

RESULTS

During the systematic evolution of ligand by exponential enrichment (SELEX) studies, we found that **ANP77** binds to RNA involving two continuous cytosines (CC) in the hairpin loop (43). Thus, we hypothesized that **ANP77** could target the internal loop of CC sites in RNA stem-loop structures. To examine the possibility, we evaluated the binding ability of **ANP77** to the internal loops of Z/CC (Z = A, C, G or U) motifs in dsRNA by melting temperature (T_m) analysis. RNA duplexes holding Z/CC sites were prepared by hybridization of two single-stranded RNA [5′-r(GUC CAG **Z** GCA ACG)-3′ and 3′-r(CAG GUC **CC** CGU UGC)-5′] and measured the T_m in the presence and absence of **ANP77** (Supplementary Figure S4). Marked stabilization of RNAs containing C/CC and U/CC sites was observed upon addition of **ANP77**, and the increased T_m (ΔT_m) was 5.8 (SD 0.1) and 4.2 (0.1)°C, respectively (Table 1, entries 1 and 2). A weak but statistically significant T_m increase of 1.3 (0.3)°C was also observed for A/CC (Table 1, entry 3). However, neither the duplexes having a single cytosine bulge (G/CC) nor the fully matched dsRNA showed such changes of T_m in the presence of **ANP77** (Table 1, entries 4 and 5), suggesting the binding of **ANP77** to these internal loops. Mass spectrometry analysis revealed that **ANP77** stabilized dsRNAs upon interaction with C/CC motifs via the formation of

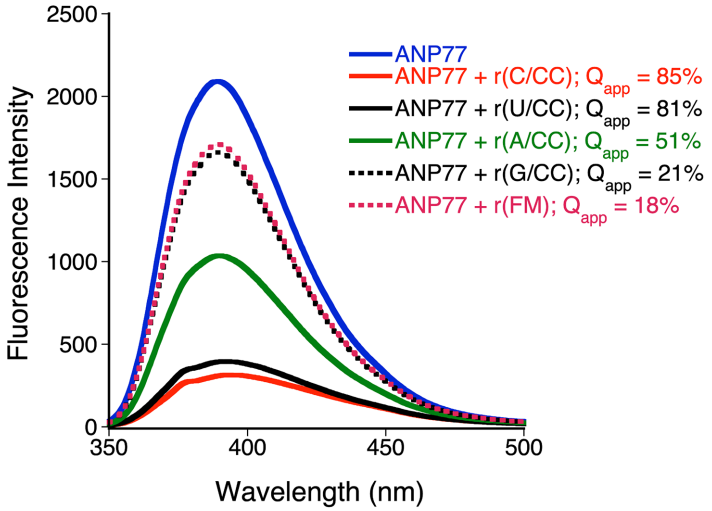

Figure 2. Fluorescence spectra (excited at 334 nm) of **ANP77** in the absence and presence of dsRNA [5′-r(GUC CAG **Z** GCA ACG)-3′ / 3′-r(CAG GUC **CC** CGU UGC)-5′] involving Z/CC motif (Z = A, C, G, or U) and a 12-mer fully matched (FM) dsRNA without Z/CC motif. Equimolar concentration (1 μM) of dsRNA and **ANP77** was used. Q_{app} represents the apparent quenching efficiency of dsRNA and were calculated based on Equation (1) described in Materials and Methods section.

Table 1. Melting temperatures of the Z/CC motif containing RNA duplexes without and with ANP77[a]

Entry	Z/CC	T_m (–)[b] (°C)	T_m (+)[c] (°C)	ΔT_m[d] (°C)
1	C/CC	50.9	56.7	5.8 (0.1)
2	U/CC	50.4	54.6	4.2 (0.1)
3	A/CC	54.0	55.3	1.3 (0.3)
4	G/CC	66.6	66.5	–0.1 (0.4)
5	-/–	69.9	69.7	–0.2 (0.3)

[a]Thermal melting curves were measured for dsRNAs [5′-r(GUC CAG **Z** GCA ACG)-3′ / 3′-r(CAG GUC **CC** CGU UGC)-5′] (5 μM) involving internal loop of Z/CC motif in 10 mM sodium cacodylate buffer (pH 7) containing 100 mM NaCl.
[b]T_m values (°C) of RNA duplexes in the absence of **ANP77**.
[c]T_m values of RNA duplexes in the presence of **ANP77** (25 μM).
[d]ΔT_m is calculated as the difference between T_m (–) and T_m (+). ΔT_m presented is the average of three independent measurements, and the standard deviations (SD) are shown in parentheses.

ANP77-r(C/CC) complex with 1:1 stoichiometry (Supplementary Figure S5). Isothermal titration calorimetry (ITC) measurements determined the binding affinity of **ANP77** to r(C/CC), r(U/CC) and r(A/CC) with the dissociation constant (K_d) of 61 nM, 69 nM and 0.70 μM, respectively, with a good fit to the 1:1 binding isotherm. The binding to A/CC is about one order of magnitude weaker compared to C/CC and U/CC (Supplementary Table S1 and Supplementary Figure S6).

Having confirmed the binding of **ANP77** to the internal loop of the Y/CC motifs in dsRNA, we then looked at the emissive properties of **ANP77** upon binding. **ANP77** showed strong fluorescence with emission (λ_{em}) maxima at 389 nm (Figure 2). Upon addition of dsRNA containing an internal loop of C/CC or U/CC site, the fluorescence of **ANP77** significantly decreased and moderately in the case of A/CC but not at the G/CC motif and 12-mer fully matched dsRNA (Figure 2). These results showed that the fluorescence of **ANP77** was markedly perturbed upon binding to dsRNA and the order of quenching efficiency is the same as that observed in T_m increase, suggesting that the intensity of **ANP77** fluorescence could be the measure of the strength of binding to C/CC, U/CC and A/CC motifs in dsRNA. A fluorometric titration between **ANP77** and dsRNA (r(C/CC)) followed by non-linear least square fitting of the data to the 1:1 binding isotherm (29) (Supplementary Figure S7) provides the *K*d of 97 nM, which is consistent of the *K*d of 61 nM determined by ITC. These results supported the good correlation between the fluorescence quenching profile with the binding to the target.

The fluorescence of **ANP77** (0.25 μM) in the bound state was examined in the presence of three RNAs, r(C/CC) (1 μM), r(U/CC) (1 μM) and r(A/CC) (2 μM). Under the conditions, the fluorescence intensity of **ANP77** bound to C/CC and U/CC RNAs were almost the same level, whereas fluorescence intensity for **ANP77** in the presence of A/CC RNA was much higher than others (Supplementary Figure S8). The **ANP77** binding to A/CC RNA obviously did not reach the saturation under the conditions, suggesting the lower affinity of **ANP77** to the A/CC RNA motif than that to the C/CC and U/CC RNAs. There are two factors affecting the degree of fluorescence quenching. The first factor is the affinity, and the other factor is the emission intensity of the bound complex. Fluorescence quenching of **ANP77** was induced by the binding to RNA, and **ANP77** exhibits different affinities depending on the RNA sequences. In this regard, the fluorescence quenching should be sequence dependent. Regarding the second factor, fluorescence of the bound complex would be also sequence dependent as the surrounding environment of fluorophore in the complex may determines the fluorescence quenching mechanism, e.g., energy transfer, electron transfer, etc. Thus, the fluorescence intensity of **ANP77** in the presence of RNA would be definitely sequence dependent.

We next looked at the effect of sequences flanking the Y/CC motif on the quenching of **ANP77** fluorescence. In the human pre-miRs registered in the miRBase database (40), the internal loop of Y/CC motifs are reasonably abun-

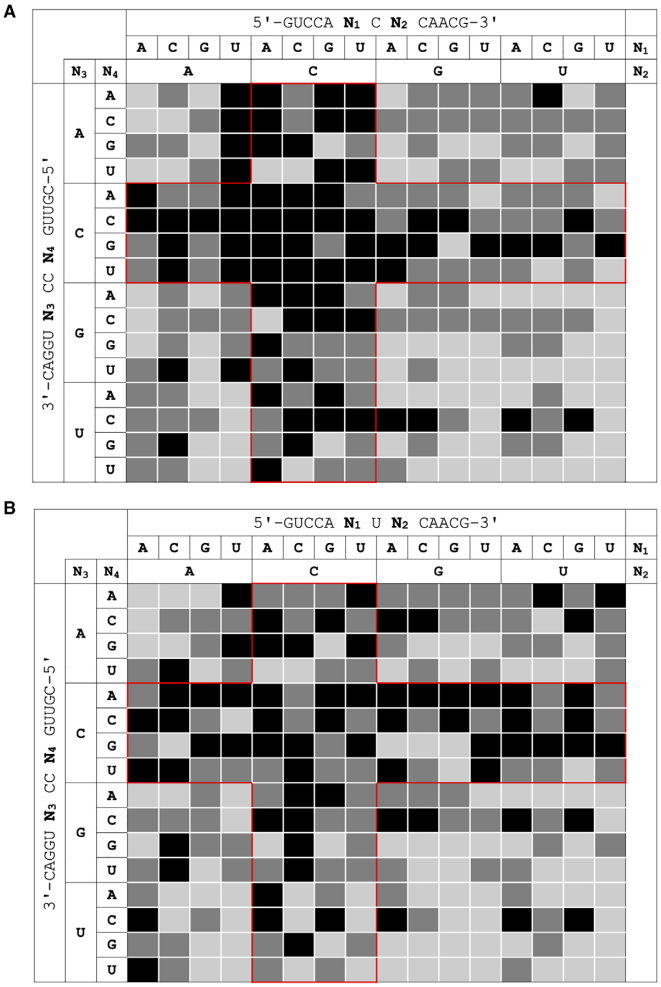

Figure 3. Heat map presentation of **ANP77** fluorescence quenching efficiency of all possible (A) C/CC (B) U/CC site flanking base paring in dsRNAs [5′-r(GUC CA $\mathbf{N_1}$Y $\mathbf{N_2}$ CA ACG)-3′ / 3′-r(CAG GU $\mathbf{N_3}$CC $\mathbf{N_4}$ GU UGC)-5′], where N_1-N_3 and N_2-N_4 are any combinations of Watson-Crick base pairs. Key: dsRNA having high quenching sequences ($Q_{app} \geq 70\%$, black boxes), moderate to good quenching sequences ($70\% > Q_{app} \geq 40\%$, grey boxes) and weak or negligible quenching sequences ($Q_{app} < 40\%$, off-white boxes).

dant with different flanking base pairs. The flanking sequence dependency for the quenching of **ANP77** fluorescence was screened with a dsRNA library containing C/CC and U/CC site flanked by all possible combinations of match and mismatch base pairs. Randomization of the flanking base pairs of C/CC and U/CC sites produces a library of 256 kinds of dsRNA (Figure 3 and Supplementary Tables S2 and S3) for each motif. Fluorometric screening of the equimolar (1 μM) mixture of **ANP77** and dsRNAs with C/CC and U/CC site using a plate reader allowed us to classify the sequences by apparent quenching efficiency (Q_{app}) into three categories: high quenching sequences ($Q_{app} \geq 70\%$, black boxes), moderate to good ($70\% > Q_{app} \geq 40\%$, grey boxes) and weak or negligible ($Q_{app} < 40\%$, off-white boxes) (Figure 3, Supplementary Tables S2 and S3). To determine the fluorescence quenching efficiency, we need to measure the fluorescence at the saturation of the binding. However, we here used Q_{app} as the classification index as we did not measure the fluorescence of **ANP77** in the fully bound state for 256 kinds of RNAs. For further discussion of FID and quenching efficiency, please see the discussion section. The screening results were cross-verified by measuring the fluorescence of the top- and bottom-ranked sequences of the C/CC (Supplementary Table S2 and Figures S9A and S10A) and U/CC sites (Supplementary Table S3 and Figures S9B and S10B) with a fluorescence spectrophotometer. The Q_{app} of four sequences are well consistent with the plate reader data (Supplementary Table S4), showing that the fluorometric screening of the dsRNA library by microplate is established.

To further gain insight into whether these quenching efficiencies of dsRNAs observed in the fluorometric screening are consistent with the binding ability to **ANP77**, we measured the melting temperature of the RNA duplexes bearing top-ranked and bottom-ranked sequences of both C/CC and U/CC sites in the presence or absence of **ANP77**. **ANP77** increased the T_m of top-ranked dsRNAs by $\geq$ 10.4°C (Supplementary Figure S9C and S9D), whereas little T_m change was observed for bottom-ranked flanking sequences (Supplementary Figure S10C and S10D), suggesting that the quenching efficiencies of dsRNAs containing C/CC and U/CC sites are the measure of binding to the **ANP77**.

Heat map analysis of the fluorometric assay data by sorting with the flanking bases showed that the highly efficient quenching sequences have a strong preference for cytosines at N_2 and N_3 positions (Figure 3 and Supplementary Figures S11 and S13). This trend is more marked for the C/CC motif than U/CC motif (Figure 3 and Supplementary Figures S12A and S14A). For the C/CC motif, out of 71 highly efficient quenching RNAs, 59 contained cytosine as the 3′ nucleotide base in one of two strands (Figure 3A, marked with red border). For the U/CC motif, 51 out of 70 contains cytosine on either of the 3′-flanking sides (Figure 3B, marked with red border). No such remarkable tendency in the flanking bases was observed for the moderate to good quenching sequences for both the motif C/CC and U/CC.

We then looked for the biologically significant and high quenching sequences involving C/CC and U/CC motifs from the miRbase database and the results were summarized in Supplementary Tables S5 and S6, respectively. To see the fluorescence change upon binding of **ANP77** to the biologically significant RNA involving the Y/CC motif, we choose the pre-miR-1908, where the C/CC internal loop exists within the Dicer processing site (Figure 4A). Dysregulation of miR-1908 has recently been reported to be associated with bipolar disorder and certain types of cancer (46,47). Addition of pre-miR-1908 to **ANP77** resulted in a significant reduction of the **ANP77** fluorescence ($Q_{app} = 72\%$) (Figure 4B), suggesting the formation of the **ANP77**-bound complex. The change in circular dichroism (CD) spectra of pre-miR-1908 in the presence of **ANP77** accompanied by the induced CD in 330–380 nm supported the complex formation (Figure 4C).

We finally demonstrated that **ANP77** could be utilized as a fluorescence indicator in the FID assay to discover small-molecule binders to the RNAs' Y/CC motif. We choose two RNA splicing modifiers known as branaplam (37)

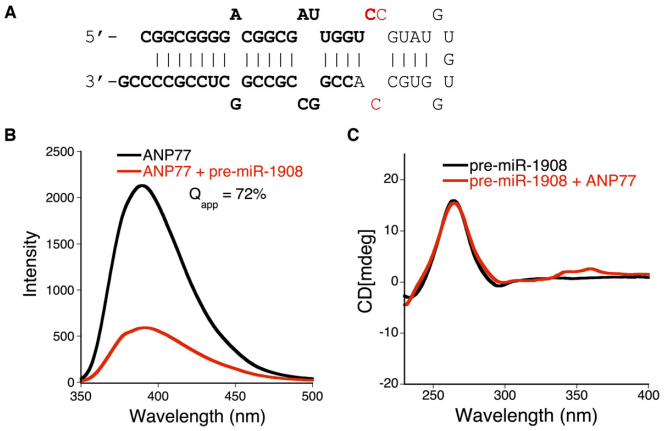

Figure 4. (**A**) Stem-loop structure of pre-miR-1908 involving internal loop of C/CC motif (red type); sequences shown in a bold type are the sequences of mature miR. (**B**) Fluorescence spectra of **ANP77** in the absence (black line) and presence (red line) of pre-miR-1908. (**C**) CD spectra of pre-miR-1908 in the absence (black line) and presence (red line) of **ANP77**.

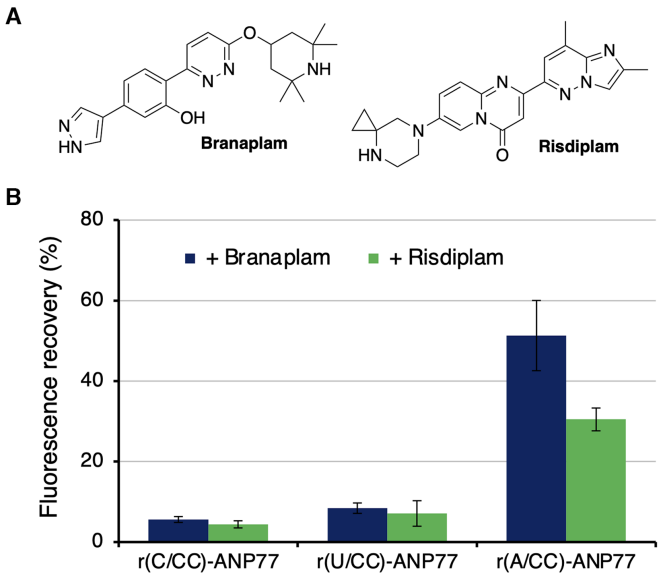

Figure 5. (**A**) Chemical structures of the drug molecules used for FID. (**B**) FID results with dsRNA involving the internal loop of Y/CC. Key: Dark blue and green represent the recovery of **ANP77** fluorescence upon the addition of branaplam and risdiplam to the **ANP77**-r(Y/CC) complex, respectively. Error bars indicate standard deviation of three independent experiments.

and risdiplam (38) as testing molecules (Figure 5A). These molecules are known to modulate RNA splicing upon interaction with the A-bulge region of the splicing site. The change of **ANP77** fluorescence in the presence of r(Y/CC) was measured with or without these compounds (Supplementary Figure S15). Upon addition of branaplam to the **ANP77**-r(Y/CC) complex, fluorescence recovery was not observed for the internal loop motif of C/CC and U/CC, but a significant increase (fluorescence recovery of about 51%) was observed for the A/CC. Risdiplam also showed a similar tendency in the fluorescence change with about 30% fluorescence recovery for A/CC RNA (Figure 5B). These results showed that branaplam and risdiplam could displace the **ANP77** bound to the A/CC site but not bound to the C/CC and U/CC sites. The recovery of **ANP77** fluorescence on r(A/CC) RNA was further evaluated by titrating **ANP77**-r(A/CC) complex with these drug molecules (Supplementary Figure S16). As the concentration of drugs increased, the fluorescence was also increased, indicating the concentration dependent displacement of **ANP77** bound to the r(A/CC) RNA. To confirm the feasibility of **ANP77**-based FID assay, we used Neomycin (6,25), a general RNA binder as a drug. Titration of preformed complex of r(Y/CC) (0.5 μM) and **ANP77** (0.25 μM) with neomycin (0–32 μM) resulted in the concentration dependent recovery of **ANP77** fluorescence (Supplementary Figure S17), showing neomycin could displace the **ANP77** bound to A/CC, C/CC and U/CC sites. Molecules screen by FID assay can be tuned in terms of the sequence selectivity and affinity by a choice of appropriate fluorescence indicators, i.e. general indicators or those with sequence selectivity. The data we presented here using **ANP77** as a sequence selective fluorescence indicator showed that RNA-binding molecules branaplam and risdiplam could not compete with **ANP77** in the binding to the C/CC and U/CC sites, but did to the A/CC site, where **ANP77** binds with weaker affinity, whereas neomycin was shown to bind to the A/CC as well as C/CC and U/CC sites.

DISCUSSION

FID assay is the method to screen out molecules binding to the target by measuring the fluorescence change of the indicator. Indicators are the fluorescence molecules binding to the target and show the fluorescence changes upon binding. To gain a high signal-to-noise ratio, the fluorescence of indicators is preferably quenched upon binding to the target, and the recovery of fluorescence from the quenched or low-level states could be observed by replacing the indicator on the target with the testing molecule. Thus, the binding of testing molecules to the target was indirectly monitored by releasing fluorescence indicators.

For the screening of molecules against one particular target, the choice of indicators would be one factor governing the successful FID screening. Figure 6A illustrated fluorescence quenching profiles of three indicators (x, y and z) with one target. The vertical axis is the normalized fluorescence intensity, whereas the horizontal axis is the concentration of the target. In this simulation, three indicators showed fluorescence changes in the different concentration range depending on the affinity of the indicator to the target, and fluorescence decreases with the increased concentration of the target. The observed fluorescence intensity (F_{obs}) with the target is described by Equation (4), where F_0 and F_{sat} is the fluorescence intensity in the absence of target and at the saturation of indicator binding to the target, respectively, and α ($0 \leq \alpha \leq 1$) is the fraction of the indicator bound to the target.

$$F_{obs} = F_0 - \alpha \cdot (F_0 - F_{sat}) \quad (4)$$

The quenching efficiency (Q) (%), termed as the fraction of decreased fluorescence, could be equal to α, if the indicator binding to the target is the predominant pathway for the

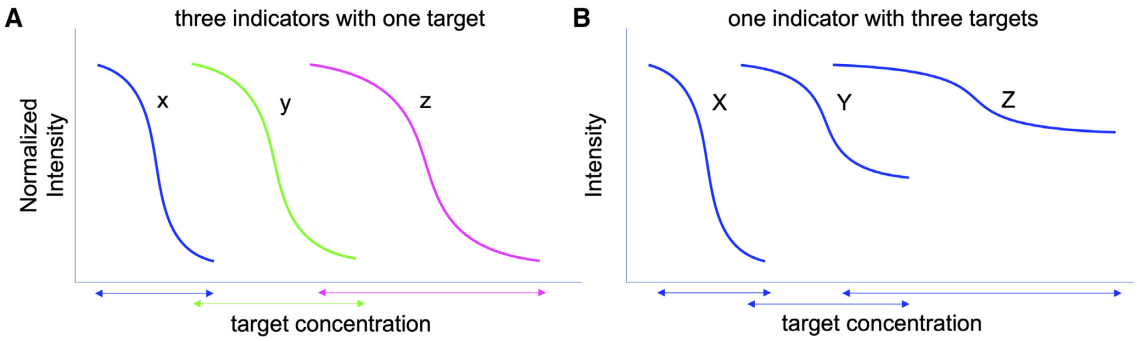

Figure 6. Illustration of simulated fluorescence quenching profiles for the case of (**A**) three indicators (*x*, *y* and *z*) with one target and (**B**) one indicator with three targets (*X*, *Y* and *Z*). The vertical axis is normalized intensity for (A) and intensity for (B). The horizontal axis is the concentration of target(s). The double headed arrows show the applicable concentration range of target(s) for FID assay.

fluorescence quenching. The FID assay implicitly adopts this assumption. It is important to note that the bound fraction α, thus the quenching efficiency Q, could be obtained if F_{sat} were measured.

$$Q = \alpha \times 100\,(\%) \tag{5}$$

The fluorescence quenching profile of indicators showed the applicable range of target concentration for the FID assay. The bound fraction of the indicator is the function of the affinity of the indicator to the target and the concentrations of indicator and target. Due to the necessary displacement of indicator bound to the target by the testing molecules, the affinity of the molecules screened out by FID assay would be explicitly determined by the affinity of the indicator. Therefore, using the several indicators with different affinities to the target covering the concentration range of interest would be the strategy of successful FID screening.

Figure 6B illustrates the quenching profiles of one indicator with three targets (*X*, *Y* and *Z*). Affinity of the indicator to targets and, therefore, the quenching profile could be different for every target. The screening of high quenching RNA motifs with one particular indicator, **ANP77,** described in Figure 3, categorized into this simulated case. RNAs showing highly effective quenching would be suitable for the FID assay as the signal-to-noise ratio would be high. We classified RNA motifs into three categories about the quenching efficiency. As we did not determine the F_{sat} for each RNA motif, the apparent quenching efficiency (Q_{app}) described by Equation (1) was used instead of Q. Under the appropriate experimental setting, F_{blank} is not significantly different between the devices and apparatus.

As illustrated in Figure 6B, it is reasonable to assume that F_{sat} could be target-dependent (sequence-dependent in these studies). Therefore, at least two possibilities should be considered for RNA motifs classified into the medium and low Q_{app}: one is the weak affinity of **ANP77** to the RNA motif, and the other is the high F_{sat} value for the **ANP77**-RNA complex than F_{blank}. The first case is the general understanding of the observed weak fluorescence quenching in the small-molecule interaction to RNA, and these RNAs are not suitable for FID assay. However, in the latter case, the RNA motifs can be applicable for the FID assay if F_{sat} was separately determined by fluorescence titration with indicator, although the dynamic range of fluorescence change would be narrow.

In FID assay, the dynamic range of the indicator fluorescence change would determine the quality of the assay. Statistically, quality of the assay could be assessed by calculating the Z'-factor (44,45), which is a measure of signal variation, here the fluorescence signal of the indicator **ANP77** in the RNA-bound and free state. Z'-factor also determines the quality of the instrumentation used in the assay. Calculating the Z'-factor for all the RNAs' used in the FID experiment with fluorescence spectrophotometer described in Figure 5 showed values of 0.49 for A/CC, 0.61 for U/CC and 0.71 for C/CC. Z'-factors range from 0 to 1, and values > 0.5 describe reliable and high-quality (44,45). To assess the quality of FID assay using fluorescence plate reader for the future assay, we utilized the 384 well plate considering the fluorescence of **ANP77** (1 μM) as high-value signal and mixture of **ANP77** and r(C/CC) (1 μM each) as low-value signal and estimated Z'-factor. The determined Z'-factor of 0.66 (cf. 0.71 with spectrophotometer) suggests that the FID assay with plate reader would be valid.

CONCLUSION

In conclusion, we reported the fluorescence properties of **ANP77** selectively binding to the internal loop of the C/CC and U/CC motifs in dsRNA. The quenching efficiency of **ANP77** fluorescence was highly dependent on the flanking bases of these motifs. The quenching phenomena of **ANP77** fluorescence was confirmed with intrinsic potential drug target pre-miR-1908. These site-specific binding of **ANP77** could be utilized as a useful modulator of RNA functions targeting Y/CC motifs and as a probe to detect sequence selective RNA–ligand interaction. We demonstrated here two RNA-binding molecules branaplam and risdiplam can displace **ANP77** at the A/CC site, where **ANP77** binds with weaker affinity than to the C/CC and U/CC sites. These studies suggest that **ANP77** would be a useful fluorescence indicator for the FID assay in screening molecules binding to the biologically significant RNA motifs of Y/CC. The binding of **ANP77** to the C/CC and U/CC sites is high in affinity which might limit the detection of moderate or weak RNA–ligand interaction, but further development of **ANP77** derivatives with lower affinity by modify-

ing the chemical structure without compromising the sequence selectivity would expand the applicable sequences for the screening of RNA-binding molecules. The screening of potential binding sites of the particular molecule (e.g. branaplam and risdiplam) would also be in the scope of FID assay using **ANP77** as a selective fluorescence indicator.

SUPPLEMENTARY DATA

Supplementary Data are available at NAR Online.

FUNDING

This work was supported by JSPS KAKENHI Grant-in-Aid for Specially Promoted Research [26000007] and for Scientific Research (A) [19H00924] for KN. Funding for open access charge: JSPS KAKENHI Grant-in-Aid for Scientific Research (A) [19H00924].
Conflict of interest statement. None declared.

REFERENCES

1. Cooper,T.A., Wan,L. and Dreyfuss,G. (2009) RNA and disease. *Cell*, **136**, 777–793.
2. Esteller,M. (2011) Non-coding RNAs in human disease. *Nat. Rev. Genet.*, **12**, 861–874.
3. Connelly,C.M., Moon,M.H. and Schneekloth,J.S. (2016) The emerging role of RNA as a therapeutic target for small molecules. *Cell Chem. Biol.*, **23**, 1077–1090.
4. Crooke,S.T., Witztum,J.L., Bennett,C.F. and Baker,B.F. (2018) RNA-targeted therapeutics. *Cell Metab.*, **27**, 714–739.
5. Yu,A.M., Choi,Y.H. and Tu,M.J. (2020) RNA drugs and RNA targets for small molecules: principles, progress, and challenges. *Pharmacol. Rev.*, **72**, 862–898.
6. Thomas,J.R. and Hergenrother,P.J. (2008) Targeting RNA with small molecules. *Chem. Rev.*, **108**, 1171–1224.
7. Warner,K.D., Hajdin,C.E. and Weeks,K.M. (2018) Principles for targeting RNA with drug-like small molecules. *Nat. Rev. Drug Discov.*, **17**, 547–558.
8. Di Giorgio,A. and Duca,M. (2019) Synthetic small-molecule RNA ligands: future prospects as therapeutic agents. *Med. Chem. Commun.*, **10**, 1242–1255.
9. Meyer,S.M., Williams,C.C., Akahori,Y., Tanaka,T., Aikawa,H., Tong,Y., Childs-Disney,J.L. and Disney,M.D. (2020) Small molecule recognition of disease-relevant RNA structures. *Chem. Soc. Rev.*, **49**, 7167–7199.
10. Hermann,T. (2018) Viral RNA targets and their small molecule ligands. *Top. Med. Chem.*, **27**, 111–134.
11. Hermann,T. (2005) Drugs targeting the ribosome. *Curr. Opin. Struct. Biol.*, **15**, 355–366.
12. Wong,C.H., Nguyen,L., Peh,J., Luu,L.M., Sanchez,J.S., Richardson,S.L., Tuccinardi,T., Tsoi,H., Chan,W.Y., Chan,H.Y.E. *et al.* (2014) Targeting toxic RNAs that cause myotonic dystrophy type 1 (DM1) with a bisamidinium inhibitor. *J. Am. Chem. Soc.*, **136**, 6355–6361.
13. Childs-Disney,J.L., Yildirim,I., Park,H., Lohman,J.R., Guan,L., Tran,T., Sarkar,P., Schatz,G.C. and Disney,M.D. (2014) Structure of the myotonic dystrophy type 2 RNA and designed small molecules that reduce toxicity. *ACS Chem. Biol.*, **9**, 538–550.
14. Winter,J., Jung,S., Keller,S., Gregory,R.I. and Diederichs,S. (2009) Many roads to maturity: microRNA biogenesis pathways and their regulation. *Nat. Cell Biol.*, **11**, 228–234.
15. Ha,M. and Kim,V.N. (2014) Regulation of microRNA biogenesis. *Nat. Rev. Mol. Cell Biol.*, **15**, 509–524.
16. Li,Y. and Kowdley,K.V. (2012) MicroRNAs in common human diseases. *Genomics Proteomics Bioinforma*, **10**, 246–253.
17. Velagapudi,S.P., Vummidi,B.R. and Disney,M.D. (2015) Small molecule chemical probes of microRNA function. *Curr. Opin. Chem. Biol.*, **24**, 97–103.
18. Jayaraj,G.G., Nahar,S. and Maiti,S. (2015) Nonconventional chemical inhibitors of microRNA: therapeutic scope. *Chem. Commun.*, **51**, 820–831.
19. Van Meter,E.N., Onyango,J.A. and Teske,K.A. (2020) A review of currently identified small molecule modulators of microRNA function. *Eur. J. Med. Chem.*, **188**, 112008.
20. Zhang,J., Umemoto,S. and Nakatani,K. (2010) Fluorescent indicator displacement assay for ligand-RNA interactions. *J. Am. Chem. Soc.*, **132**, 3660–3661.
21. Watkins,D., Norris,F.A., Kumar,S. and Arya,D.P. (2013) A fluorescence-based screen for ribosome binding antibiotics. *Anal. Biochem.*, **434**, 300–307.
22. Wicks,S.L. and Hargrove,A.E. (2019) Fluorescent indicator displacement assays to identify and characterize small molecule interactions with RNA. *Methods*, **167**, 3–14.
23. Meyer,S.T. and Hergenrother,P.J. (2009) Small molecule ligands for bulged RNA secondary structures. *Org. Lett.*, **11**, 4052–4055.
24. Pei,R. and Stojanovic,M.N. (2008) Study of thiazole orange in aptamer-based dye-displacement assays. *Anal. Bioanal. Chem.*, **390**, 1093–1099.
25. Asare-Okai,P.N. and Chow,C.S. (2011) A modified fluorescent intercalator displacement assay for RNA ligand discovery. *Anal. Biochem.*, **408**, 269–276.
26. Hamasaki,K. and Rando,R.R. (1998) A high-throughput fluorescence screen to monitor the specific binding of antagonists to RNA targets. *Anal. Biochem.*, **261**, 183–190.
27. Lee,E.T.T., Sato,Y. and Nishizawa,S. (2020) Small molecule-PNA oligomer conjugates for rRNA A-site at neutral pH for FID assays. *Chem. Commun.*, **56**, 14976–14979
28. Murata,A., Nakamori,M. and Nakatani,K. (2019) Modulating RNA secondary and tertiary structures by mismatch binding ligands. *Methods*, **167**, 78–91.
29. Umemoto,S., Im,S., Zhang,J., Hagihara,M., Murata,A., Harada,Y., Fukuzumi,T., Wazaki,T., Sasaoka,S.I. and Nakatani,K. (2012) Structure-activity studies on the fluorescent indicator in a displacement assay for the screening of small molecules binding to RNA. *Chem. Eur. J.*, **18**, 9999–10008.
30. Zhang,J., Takei,F. and Nakatani,K. (2007) Emission of characteristic fluorescence from the ligand-cytosine complex in U_A/ACU bulged RNA duplex. *Bioorg. Med. Chem.*, **15**, 4813–4817.
31. Shibata,T. and Nakatani,K. (2016) Fluorescence probe for detecting CCG trinucleotide repeat DNA expansion and slip-out. *ChemBioChem*, **17**, 1685–1688.
32. Fukuzumi,T., Murata,A., Aikawa,H., Harada,Y. and Nakatani,K. (2015) Exploratory study on the RNA-binding structural motifs by library screening targeting pre-MiRNA-29a. *Chem. Eur. J.*, **21**, 16859–16867.
33. Murata,A., Harada,Y., Fukuzumi,T. and Nakatani,K. (2013) Fluorescent indicator displacement assay of ligands targeting 10 microRNA precursors. *Bioorg. Med. Chem.*, **21**, 7101–7106.
34. Murata,A., Otabe,T., Zhang,J. and Nakatani,K. (2016) BzDANP, a small-molecule modulator of pre-MiR-29a maturation by Dicer. *ACS Chem. Biol.*, **11**, 2790–2796.
35. Otabe,T., Nagano,K., Kawai,G., Murata,A. and Nakatani,K. (2019) Inhibition of pre-miRNA-136 processing by Dicer with small molecule BzDANP suggested the formation of ternary complex of pre-miR-136–BzDANP–Dicer. *Bioorg. Med. Chem.*, **27**, 2140–2148.
36. Kobori,A., Horie,S., Suda,H., Saito,I. and Nakatani,K. (2004) The SPR sensor detecting cytosine-cytosine mismatches. *J. Am. Chem. Soc.*, **126**, 557–562.
37. Palacino,J., Swalley,S.E., Song,C., Cheung,A.K., Shu,L., Zhang,X., Van Hoosear,M., Shin,Y., Chin,D.N., Keller,C.G. *et al.* (2015) SMN2 splice modulators enhance U1-Pre-mRNA association and rescue SMA mice. *Nat. Chem. Biol.*, **11**, 511–517.
38. Ratni,H., Ebeling,M., Baird,J., Bendels,S., Bylund,J., Chen,K.S., Denk,N., Feng,Z., Green,L., Guerard,M. *et al.* (2018) Discovery of risdiplam, a selective survival of motor neuron-2 (SMN2) gene splicing modifier for the treatment of spinal muscular atrophy (SMA). *J. Med. Chem.*, **61**, 6501–6517.
39. Risdiplam recently approved by US Food and Drug Administration (FDA) and Branaplam entered in clinical trials, Singh,R.N., Ottesen,E.W. and Singh,N.N. (2020) The first orally deliverable small molecule for the treatment of spinal muscular atrophy. *Neurosci. Insights*, **15**, 2633105520973985.

40. Kozomara,A., Birgaoanu,M. and Griffiths-Jones,S. (2019) miRBase: from microRNA sequences to function. *Nucleic Acids Res.*, **47**, D155–D162.
41. Costales,M.G., Haga,C.L., Velagapudi,S.P., Childs-Disney,J.L., Phinney,D.G. and Disney,M.D. (2017) Small molecule inhibition of microRNA-210 reprograms an oncogenic hypoxic circuit. *J. Am. Chem. Soc.*, **139**, 3446–3455.
42. Arachchilage,G.M., Kharel,P., Reid,J. and Basu,S. (2018) Targeting of G-quadruplex harboring Pre-miRNA 92b by LNA rescues PTEN expression in NSCL cancer cells. *ACS Chem. Biol.*, **13**, 909–914.
43. Nakatani,K., Natsuhara,N., Mori,Y., Mukherjee,S., Das,B. and Murata,A. (2017) Synthesis of naphthyridine dimers with conformational restriction and binding to DNA and RNA. *Chem. Asian J.*, **12**, 3077–3087.
44. Zhang,J.H., Chung,T.D.Y. and Oldenburg,K.R. (1999) A simple statistical parameter for use in evaluation and validation of high throughput screening assays. *J. Biomol. Screening*, **4**, 67–73.
45. Birmingham,A., Selfors,L.M., Forster,T., Wrobel,D., Kennedy,C.J., Shanks,E., Santoyo-Lopez,J., Dunican,D.J., Long,A., Kelleher,D. *et al.* (2009) Statistical methods for analysis of high-throughput RNA interference screens. *Nat. Methods*, **6**, 569–575.
46. Forstner,A.J., Hofmann,A., Maaser,A., Sumer,S., Khudayberdiev,S., Mühleisen,T.W., Leber,M., Schulze,T.G., Strohmaier,J., Degenhardt,F. *et al.* (2015) Genome-wide analysis implicates MicroRNAs and their target genes in the development of bipolar disorder. *Transl. Psychiatry*, **5**, e678.
47. Xia,X., Li,Y., Wang,W., Tang,F., Tan,J., Sun,L., Li,Q., Sun,L., Tang,B. and He,S. (2015) MicroRNA-1908 functions as a glioblastoma oncogene by suppressing PTEN tumor suppressor pathway. *Mol. Cancer*, **14**, 154.